Storm surge characteristics and extreme parameters in the Chengshantou sea area

Y D Jin[1,2], X Zhao[1] and L N Ma[1]

[1]First Institute of Oceanography, SOA, Qingdao 266061, China

E-mail: jyd@fio.org.cn

Abstract. Storm surge in the Chengshantou sea area is simulated by the advanced circulation (ADCIRC) model. The Regional Atmospheric Modeling System (RAMS) wind model is used to simulate wind parameters used to be wind force of storm surge model. The comparison results of storm surges show good agreement between simulations and observations. The storm surge is caused by typhoon in summer but extratropical cyclone in winter. By statistical analysis of storm surge in 20 years, it is found that the annual max negative storm surge are all caused by extratropical cyclone while the frequency of annual max positive storm surge caused by tropical cyclone is about 20%. The extreme parameters are estimated by Gumbel distribution. The positive extreme storm surge of 100 year return period is determined as 95 cm and the negative is -124 cm.

1. Introduction

Recent advances have provided new tools for modeling storm surges in estuarine and coastal sea areas. The advanced circulation (ADCIRC) model incorporates a good combination of these three elements, making storm surge simulation one of its main applications [1]. Androulidakis *et al* [2] explored the trends of storm surge extremes in the Mediterranean Sea for a period of 150 years (1951–2100) by using a high-resolution storm surge model. Tomkratoke *et al* [3] used a numerical simulation to determine the effective resonance period, quality factor Q and linear friction coefficient and mechanism of tide and storm surge in the Gulf of Thailand. Lawler *et al* [4] investigated the impact of spatial scaling, mesh resolution, storm characteristics and bottom friction on storm surge in wetland areas in the barrier island system of the Delmarva Peninsula using the coupled hydrodynamic-wave model (ADCIRC+SWAN). Soomere & Pindsoo [5] addressed the possibilities of a separation of the overall increasing trend in maximum water levels of semi-enclosed water bodies into associated trends in the heights of local storm surges and basin-scale components of the water level based on recorded and modeled local water level time series. Mo *et al* [6] developed a three-dimensional numerical model to study storm surges induced by cold waves. Yin *et al* [7] investigated the effects of potential sea level rise as well as typhoon intensification (TI) on storm surges through the use of coupled ADCIRC+SWAN models. Lewis *et al* [8] presented the first assessment of the potential impact of storm surges on tidal-range power. Krien *et al* [9] made use of a state-of-the art numerical modeling system with improved bathymetric and topographic data to identify the strengths, weaknesses, and to suggest areas for improvement of current storm surge models in northern Bay of Bengal.

Chengshan is located in the coastal area of the east of Shandong Peninsula (figure 1), facing the Yellow Sea. It is the storm more serious areas in the north of China. The purpose of this paper is to study the characteristics of storm surge in Chengshantou Sea by means of numerical simulation, and to

provide scientific support for disaster prevention and mitigation in this area. The paper is divided into 4 parts. Numerical simulation is applied in section 2. Section 3 is the results and discussion. Finally, the conclusion is given in section 4.

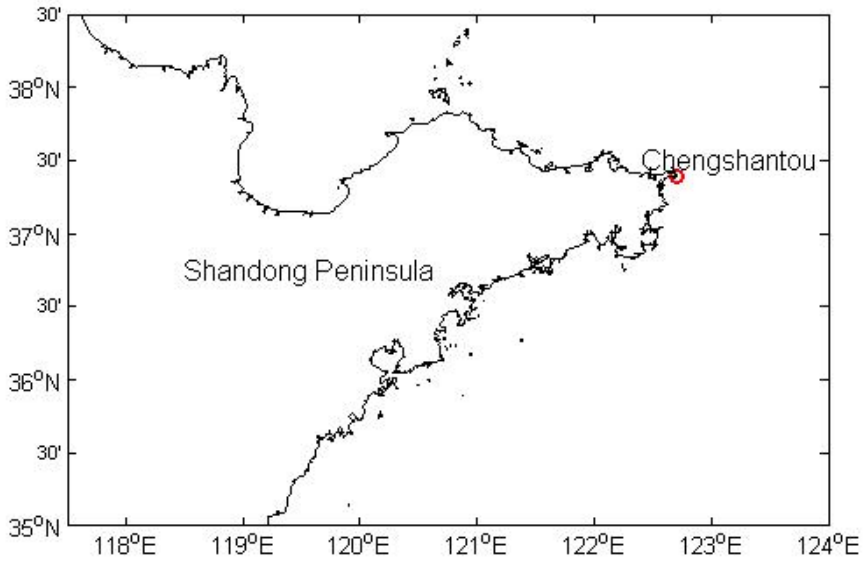

Figure 1. Location of Chengshantou.

2. Numerical simulation

2.1. Model description

The advanced circulation (ADCIRC) model is a highly-developed computer program for oceanic, coastal, and estuarine waters. All nonlinear terms have been retained in these equations and ADCIRC can be run with either a spherical coordinate or Cartesian system, both of which make ADCIRC preferred to some other storm surge models. The two-dimensional governing equations for storm surge in Cartesian coordinates are the Primitive continuity equation:

$$\frac{\partial \zeta}{\partial t} + \frac{\partial UH}{\partial x} + \frac{\partial VH}{\partial y} = 0 \tag{1}$$

and the Primitive momentum equations:

$$\frac{\partial U}{\partial t} + U\frac{\partial U}{\partial x} + V\frac{\partial U}{\partial y} - fV = -\frac{\partial}{\partial x}\left[\frac{p_s}{\rho_0} + g\,\zeta - g\,(\eta + \gamma)\right] + \frac{\tau_{sx}}{\rho_0 H} - \frac{\tau_{bx}}{\rho_0 H} + D_x - B_x \tag{2}$$

$$\frac{\partial V}{\partial t} + U\frac{\partial V}{\partial x} + V\frac{\partial V}{\partial y} + fU = -\frac{\partial}{\partial y}\left[\frac{p_s}{\rho_0} + g\zeta - g(\eta + \gamma)\right] + \frac{\tau_{sy}}{\rho_0 H} - \frac{\tau_{by}}{\rho_0 H} + D_y - B_y \tag{3}$$

where, x and y are the Cartesian coordinates, with east and north having positive values; u and v are the depth-averaged components of velocity in the x and y direction, respectively; t is the time; f is the Coriolis parameter; ρ_0 is water density; H is the total water depth; p_s is the atmospheric pressure on the sea surface; g is acceleration due to gravity; ζ is the elevation of the sea surface above the undisturbed water level; τ_{sx} and τ_{sy} represent the components of wind stress on the sea surface; τ_{bx} and τ_{by} represent the components of sea floor stress; and $(\eta+\gamma)$ represents the Newtonian tidal potential, earth tide, self-attraction, and load tide.

$$B_x = \frac{g}{H}\int_{-h}^{\zeta}\left[\partial/\partial x\int_{z}^{\zeta}\left(\frac{\rho-\rho_0}{\rho_0}\right)dz\right]dz \quad B_y = \frac{g}{H}\int_{-h}^{\zeta}\left[\partial/\partial y\int_{z}^{\zeta}\left(\frac{\rho-\rho_0}{\rho_0}\right)dz\right]dz \tag{4}$$

$$D_x = \frac{E_h}{H}\left[\frac{\partial^2 UH}{\partial x^2}+\frac{\partial^2 UH}{\partial y^2}\right] D_y = \frac{E_h}{H}\left[\frac{\partial^2 VH}{\partial x^2}+\frac{\partial^2 VH}{\partial y^2}\right] \tag{5}$$

$$\tau_{bx} = U\tau_*;\tau_{by} = V\tau_*;\tau_* = \frac{C_f(U^2+V^2)^{1/2}}{H} \tag{6}$$

$$\frac{\partial^2\zeta}{\partial t^2}+\tau_0\frac{\partial\zeta}{\partial t}+\frac{\partial A_x}{\partial x}+\frac{\partial A_y}{\partial y}-UH\frac{\partial\tau_0}{\partial x}-VH\frac{\partial\tau_0}{\partial y}=0 \tag{7}$$

where:

$$A_x = U\frac{\partial H}{\partial t}+H\{-U\frac{\partial U}{\partial x}-V\frac{\partial U}{\partial y}+fV-\frac{\partial}{\partial x}\left[\frac{p_s}{\rho_0}+g\zeta-g(\eta+\gamma)\right]+\frac{\tau_{sx}}{\rho_0 H}-\frac{\tau_{bx}}{\rho_0 H}+\tau_0 U+D_x-B_x\} \tag{8}$$

$$A_y = V\frac{\partial H}{\partial t}+H\{-U\frac{\partial V}{\partial x}-V\frac{\partial V}{\partial y}-fU-\frac{\partial}{\partial y}\left[\frac{p_s}{\rho_0}+g\zeta-g(\eta+\gamma)\right]+\frac{\tau_{sy}}{\rho_0 H}-\frac{\tau_{by}}{\rho_0 H}+\tau_0 V+D_y-B_y\} \tag{9}$$

2.2. Wind force and bathymetry data

The wind parameters used to simulate storm surge are simulated by the Regional Atmospheric Modeling System (RAMS [10]). The equations of RAMS are as follows:

$$\frac{\partial u}{\partial t} = -u\frac{\partial u}{\partial x}-v\frac{\partial u}{\partial y}-w\frac{\partial u}{\partial z}-\theta\frac{\partial\pi'}{\partial x}+fv+\frac{\partial}{\partial x}(k_{\mathrm{m}}\frac{\partial u}{\partial x})+\frac{\partial}{\partial y}(k_{\mathrm{m}}\frac{\partial u}{\partial y})+\frac{\partial}{\partial z}(k_{\mathrm{m}}\frac{\partial u}{\partial z}) \tag{10}$$

$$\frac{\partial v}{\partial t} = -u\frac{\partial v}{\partial x}-v\frac{\partial v}{\partial y}-w\frac{\partial v}{\partial z}-\theta\frac{\partial\pi'}{\partial y}-fu+\frac{\partial}{\partial x}(k_{\mathrm{m}}\frac{\partial v}{\partial x})+\frac{\partial}{\partial y}(k_{\mathrm{m}}\frac{\partial v}{\partial y})+\frac{\partial}{\partial z}(k_{\mathrm{m}}\frac{\partial v}{\partial z}) \tag{11}$$

$$\frac{\partial w}{\partial t} = -u\frac{\partial w}{\partial x}-v\frac{\partial w}{\partial y}-w\frac{\partial w}{\partial z}-\theta\frac{\partial\pi'}{\partial z}-\frac{g\theta_v'}{\theta_0}+\frac{\partial}{\partial x}(k_{\mathrm{m}}\frac{\partial w}{\partial x})+\frac{\partial}{\partial y}(k_{\mathrm{m}}\frac{\partial w}{\partial y})+\frac{\partial}{\partial z}(k_{\mathrm{m}}\frac{\partial w}{\partial z}) \tag{12}$$

$$\frac{\partial\theta_{\mathrm{il}}}{\partial t} = -u\frac{\partial\theta_{\mathrm{il}}}{\partial x}-v\frac{\partial\theta_{\mathrm{il}}}{\partial y}-w\frac{\partial\theta_{\mathrm{il}}}{\partial z}+\frac{\partial}{\partial x}(k_{\mathrm{h}}\frac{\partial\theta_{\mathrm{il}}}{\partial x})+\frac{\partial}{\partial y}(k_{\mathrm{h}}\frac{\partial\theta_{\mathrm{il}}}{\partial y})+\frac{\partial}{\partial z}(k_{\mathrm{h}}\frac{\partial\theta_{\mathrm{il}}}{\partial z})+(\frac{\partial\theta_{\mathrm{il}}}{\partial \mathrm{t}})_{\mathrm{rad}} \tag{13}$$

$$\frac{\partial \mathrm{r_n}}{\partial t} = -u\frac{\partial \mathrm{r_n}}{\partial x}-v\frac{\partial \mathrm{r_n}}{\partial y}-w\frac{\partial \mathrm{r_n}}{\partial z}+\frac{\partial}{\partial x}(k_{\mathrm{h}}\frac{\partial \mathrm{r_n}}{\partial x})+\frac{\partial}{\partial y}(k_{\mathrm{h}}\frac{\partial \mathrm{r_n}}{\partial y})+\frac{\partial}{\partial z}(k_{\mathrm{h}}\frac{\partial \mathrm{r_n}}{\partial z}) \tag{14}$$

$$\frac{\partial\pi'}{\partial t} = -\frac{\mathrm{R}\pi_0}{\mathrm{C_v}\rho_0\theta_0}(\frac{\partial\rho_0\theta_0 \mathrm{u}}{\partial x}+\frac{\partial\rho_0\theta_0 v}{\partial y}+\frac{\partial\rho_0\theta_0 \mathrm{w}}{\partial z}) \tag{15}$$

where, u and v represent the zonal wind vector and meridional wind vector respectively; w represents the vertical wind vector; k_m and k_h represent eddy viscosity coefficient; f represents Coriolis parameter; θ_v represents virtual potential temperature; θ_{il} represents ice-liquid water potential temperature; r_v is water vapor mixing ratio; g represents the gravity coefficient; ρ represents density; R is the gas constant; C_v is specific heat capacity and π represents total Exner function.

The RAMS model is run every hour in this study. The time range is from 1987 to 2006. The horizontal resolution of RAMS is set to 0.1° by 0.1°. There are 16 layers in the vertical directions. The Klemp/Wilhelmson scheme is used in the lateral boundary. The initial fields are NCEP reanalysis wind data which the horizontal resolution of that is 0.25° by 0.25° and the time resolution is 6 hours.

The topography datasets used in this paper are shown in figure 2. The topography datasets are derived from admiralty chart in the Bohai Sea and ETOPO5 in the Yellow Sea [11].

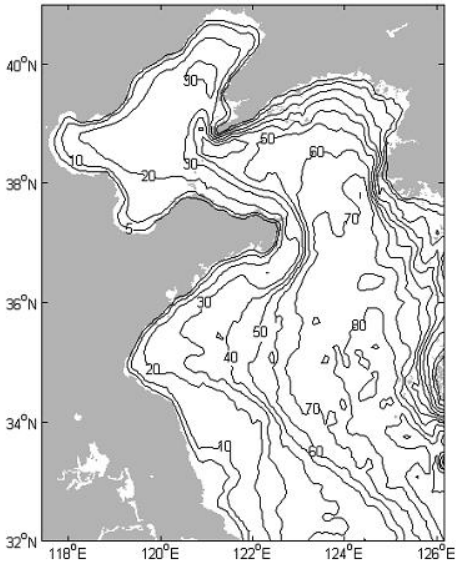

Figure 2. Depth of computational domain.

2.3. Model set-up and validation

The ADCIRC-2DDI model adopts the finite element (FE) method using triangular mesh, to improve description of the complex coastal and island boundaries. The computational domain covers approximately 8.75° longitude and 9° latitude which is from 117.4167° E to 126.1667° E and from 32° N to 41° N.

The initial condition state is set to zero including currents and surface elevation, $\zeta = U = V = 0$. The lateral boundary conditions are driven by four main astronomical tidal constituents (K_1, O_1, S_2, and M_2) along the open boundary, and are assumed to be zero when there is normal flow to the solid boundary. The sea floor stress has the parameters of a quadratic law in terms of the horizontal velocity vector at the bottom sea layer. In addition, the dry and wet method is adopted to satisfy the moving boundary; allowing veritable simulation of the process of storm surge across floodplains.

The storm surge during typhoon and extratropical cyclone are both validated. Two typhoons 8509 and 9216 are selected for data validation and the progress of extratropical cyclone is in April 1987 and February 1994 respectively. The validation results are shown in figures 3 and 4. The dotted line is the observation data in Chengshantou station and the solid line is the simulation data by ADCIRC. It could be seen that ADCIRC can simulate the storm surge well in the Chengshantou sea area.

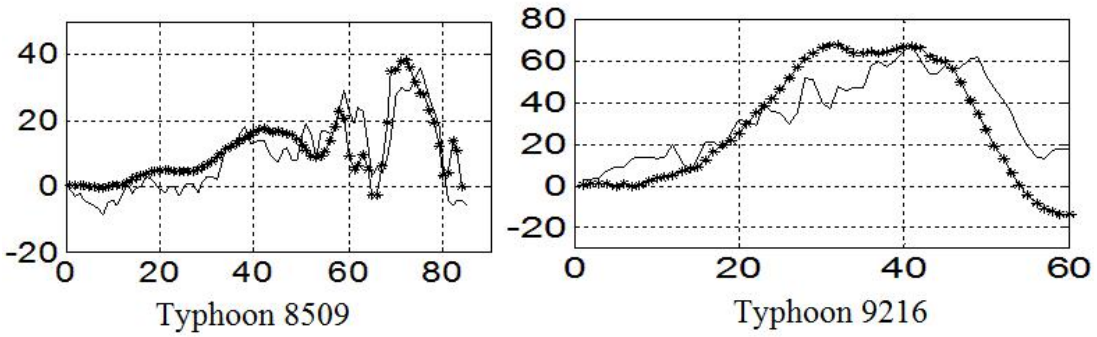

Figure 3. Storm surge validation duirng typhoon 8509 and 9216 (The dotted line is the observation data and the solid line is the simulation data).

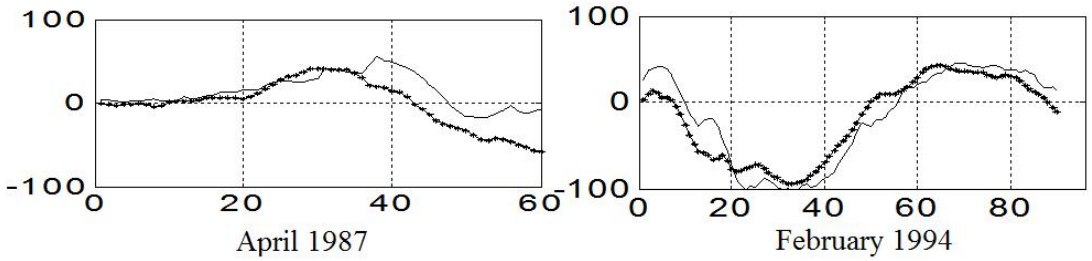

Figure 4. Storm surge validation during extratropical cyclone in 1987 and 1994 (The dotted line is the observation data and the solid line is the simulation data).

3. Results and discussion

3.1. Statistical analysis

The results show that the storm surge is caused by typhoon in summer but extratropical cyclone in winter by statistical analysis of storm surge in 20 years between 1987 and 2006. The processes of typhoon occur in late July, August and September each year while the extratropical cyclone usually happens in January, February and December. Frontal system is the most important weather system in eastern Shandong. Storm surge caused by frontal system generally appears in the spring, autumn and winter. Among those, the max value of negative storm surge caused by frontal system usually happens from January to April.

The annual extreme values of positive and negative storm surge between 1987 and 2006 are shown in figure 5. The red circle indicates the storm caused by the tropical cyclone. There are four years which the extreme values of positive storm surge are caused by tropical cyclone. The frequency is about 20%. On the other hand, the annual extreme values of negative storm surge are all caused by extratropical cyclone.

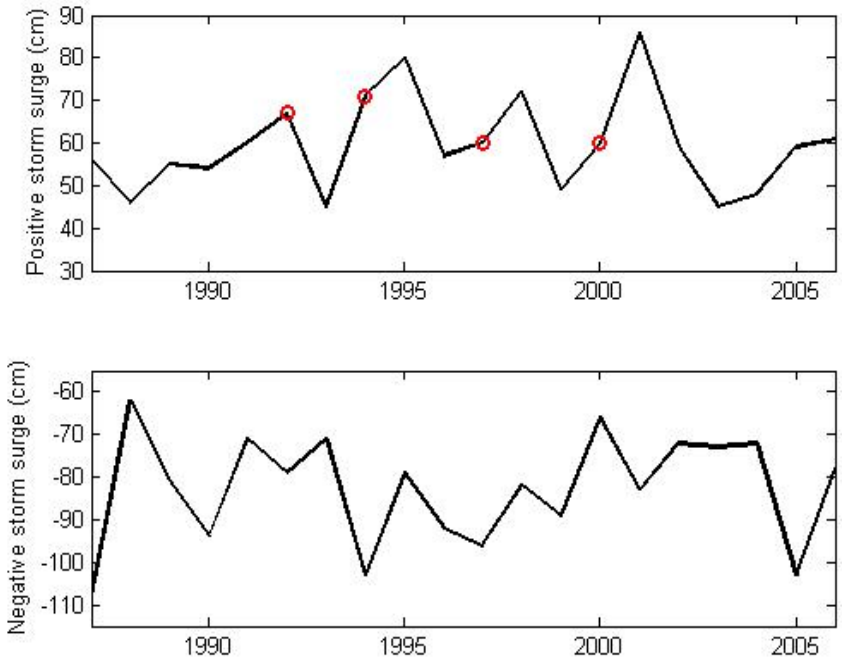

Figure 5. The annual extreme values of positive and negative storm surge between 1987 and 2006.

3.2. Extreme parameter

The extreme parameters of storm surge are estimated by three methods which are Weibull, Gumbel and P-III distribution. The biggest advantage of P-III distribution is its high elasticity. The theoretical curve and empirical frequency points could be fit well by curve fitting or adjust the deviation coefficient and mean value. The disadvantage is the optional arbitrarily increase when the data sequence is short especially there are several same values in the statistical sample. The probability density function of P-III distribution is as follows,

$$f(x)=\frac{\beta^{\alpha}}{\Gamma(\alpha)}(x-a_0)^{\alpha-1}e^{-\beta(x-a_0)},\ x\geq a_0,\quad \alpha>0 \tag{16}$$

Where a_0 is the location parameter; α is the shape parameter and β is the scale parameter.

The Weibull distribution is derived from the combination of theory and empirical data. There are three (or two) dependent parameters of the sample in its distribution. The application of Weibull distribution is more flexible. The slope and intercept of those parameters can be directly from the probability map, or could be got by least square method. The location parameter is usually obtained by the successive approximation method. The probability density function of P-III distribution is as follows,

$$f\left(x\right)=\frac{\alpha}{\beta}\left(x-a_0\right)^{\alpha-1}\exp\left[-\frac{\left(x-a_0\right)^{\alpha}}{\beta}\right]\quad x\geq a_0 \tag{17}$$

The Gumbel distribution is the first type of distribution derived from the extreme distribution theory. The greatest advantage of this distribution is that the theory is based on fullness, no arbitrariness, and the degree of fit near the median is better. The disadvantage is it is difficult to treat the problem of singular extreme value. When the max value of sample Xmax is less than the specific value x, the distribution function of Gumbel distribution is as follows,

$$F(x)=P\left\{X_{\max}<x\right\}=\exp\left[-\exp(-\frac{x-\mu}{\sigma})\right] \tag{18}$$

The extreme parameters of storm surge are estimated by the above statistical methods using the annual extreme positive and negative data. The results of 100 year return period are shown in table 1.

Table 1. The positive and negative storm surge of 100 year return period.

	Weibull	Gumbel	PIII
Positive storm surge	86	95	94
Negative storm surge	-113	-124	-121

It could be found that the positive storm surge estimated by Gumbel distribution is the largest in these three methods with the value 95 cm. The nest is that estimated by P-III distribution with the value 1 cm less than Gumbel distribution. On the other hand, the negative storm surge estimated by Gumbel distribution is the largest in these three methods with the value -124 cm. The nest is that estimated by P-III distribution with the value 3cm less than Gumbel distribution. The results of the Weibull distribution are generally smaller than those of the other two methods. From a conservative and security perspective, the positive extreme storm surge of 100 year return period is determined as 95 cm and the negative is -124 cm. All the values are estimated by Gumbel distribution.

4. Conclusion

This study presents a study on storm surge characteristics and extreme parameters in the Chengshantou sea area. The storm surges are simulated by ADCIRC from 1987 to 2006 with model

input of wind force from RAMS. Comparisons of storm surge between simulations and observations show good agreement.

Results show that there are four years which the annual max positive storm surges are caused by tropical cyclone. The frequency is about 20%. The annual max negative storm surges are all caused by extratropical cyclone. The positive extreme storm surge of 100 year return period is determined as 95cm and the negative is -124 cm. All the values are estimated by Gumbel distribution.

In brief, this paper increases the understanding of storm surge in the Chengshantou. It is useful and helpful for marine engineering and disaster prevention and mitigation.

References

[1] Wu Y N, Wang Z F, Dong S, Li J J 2014 Numerical simulation and statistic analysis of typhoon storm surge in the sea area around Shandong Peninsula *Proc. of the Eleventh (2014) Pacific/Asia Offshore Mechanics Symposium* (Shanghai, China) 10 12-6

[2] Androulidakis Y S, Kombiadou K D, Makris C V, Baltikas V N and Krestenitis Y N 2015 Storm surges in the mediterranean sea: Variability and trends under future climatic conditions *Dynam. Atmos. Oceans* **71** 56-82

[3] Tomkratoke S, Sirisup S, Udomchoke V and Kanasut J 2015 Influence of resonance on tide and storm surge in the gulf of thailand *Cont. Shelf Res.* **109** 112-26

[4] Lawler S, Haddad J and Ferreira C M 2016 Sensitivity considerations and the impact of spatial scaling for storm surge modeling in wetlands of the mid-atlantic region *Ocean Coastal Manage.* **134** 226-38

[5] Soomere T and Pindsoo K 2016 Spatial variability in the trends in extreme storm surges and weekly-scale high water levels in the eastern baltic sea *Cont. Shelf Res.* **115** 53-64

[6] Mo D, Hou Y, Li J and Liu Y 2016 Study on the storm surges induced by cold waves in the northern east china sea *J. Marine Syst.* **160** 26-39

[7] Yin K, Xu S D, Huang W R and Xie Y 2017 Effects of sea level rise and typhoon intensity on storm surge and waves in Pearl River Estuary *Ocean Eng.* **136** 80-93

[8] Lewis M J, Angeloudis A, Robins P E, Evans P S and Neill S P 2017 Influence of storm surge on tidal range energy *Energy* **122** 25-36

[9] Krien Y, Testut L, Islam A K M S, Bertin X, Durand F, Mayet C and Ballu V 2017 Towards improved storm surge models in the northern Bay of Bengal *Cont. Shelf Res.* **135** 58-73

[10] Wang Z F, Dong S, Li X and Guedes S C 2016 Assessments of wave energy in the Bohai Sea China *Renew. Energ.* **90** 145-56

[11] Wang Z F, Dong S, Chen C C and Guedes S C 2015 Long-term characteristics and extreme parameters of currents and sea levels in the Bohai Sea based on 20-year numerical hindcast data *Nat. Hazards* **76** 1603-24